

peaks at 59.7 (epoxide ^{13}C), 69.6 (^{13}C -OH), and 129.3 (sp^2C) parts per million (ppm) in Fig. 3A are based on studies by Lerf *et al.* (23). We performed additional analyses and confirmed that these assignments are likely correct (21). The obtained 1D spectrum shows similar features with those reported in (23) except for the relatively well-resolved minor peaks at 101, 169, and 193 ppm, which respectively yield only 12%, 15%, and 4% of the integrated intensity of the 70-ppm peak. The spectrum shows a considerably stronger sp^2 peak and a much weaker peak at 169 ppm compared with that by Szabo *et al.* (22), although the observed peak positions are similar. The peak at 169 ppm was previously attributed to $^{13}\text{C}=\text{O}$ (22). The results imply that their sample was subject to a higher level of oxidization than ours.

Because the natural abundance of ^{13}C is only 1%, attaining sufficient sensitivity in a 2D spectrum, as shown in Fig. 3B, is extremely difficult without the ^{13}C -labeled samples. For example, ^{13}C - ^{13}C bonds exist only at 0.01% abundance without labeling; thus, obtaining an equivalent 2D spectrum for an unlabeled sample would require about 10^8 times as much time. The experiment in Fig. 3B was performed with a finite-pulse radio frequency-driven dipolar recoupling (fpRFDR) mixing sequence (24). With the labeled sample and a relatively short mixing time (1.6 ms), the experiment permitted us to identify ^{13}C - ^{13}C pairs directly bonded or separated by two bonds. In Fig. 3B, there are several strong cross peaks. For example, cross peaks were observed at the positions $(\omega_1, \omega_2) = (133 \text{ ppm}, 70 \text{ ppm})$ and $(130 \text{ ppm}, 59 \text{ ppm})$ (green signals in Fig. 3B). These cross peaks represent spin polarization transfer from sp^2 carbons observed at ~ 130 ppm in ω_1 , to C-OH and epoxide groups, which appear at 70 ppm and 59 ppm in ω_2 , respectively. Unlike previous studies, these cross peaks directly present the connectivity between sp^2C and ^{13}C -OH, as well as that between sp^2 and epoxide ^{13}C through spin-spin dipolar couplings. The cross peak intensities are about 10%, compared with the diagonal signals, which represent signals for ^{13}C spins that had the same NMR frequencies in the two dimensions ($\omega_1 = \omega_2$). The relatively strong intensities of the cross peaks suggest that a large fraction of the sp^2C atoms are directly bonded to ^{13}C -OH and/or epoxide ^{13}C .

We also observed strong cross peaks between ^{13}C -OH and ^{13}C -epoxide (red signals). Again, the data suggest that a large fraction of C-OH and epoxide carbons are bonded to each other. The blue cross peaks indicate that there are sp^2 species having slightly different chemical shifts and that they are bonded with each other. Indeed, the sp^2C shifts for the cross peaks (green) are slightly different for the cross peaks to C-OH (133 ppm) and that to epoxide (130 ppm).

In the previous studies (23), the proximities of the chemical groups were tentatively assigned based on formation of the phenol group during the deoxidization of GO. In contrast, the present SSNMR data directly shows that these groups are chemically bonded. For the minor species, we

found cross peaks only for the peak at 101 ppm (orange box). There are no visible cross peaks for the other minor components at 169 and 193 ppm, despite these minor peaks having comparable intensities to the 101-ppm peak. The results imply that these minor components at 169 and 193 ppm, which were previously attributed to the presence of C=O (2, 22), are spatially separated from a majority of the sp^2 , C-OH, and epoxide carbons.

Among six previously proposed models (22), only two, the Lerf-Klinowski model (23) and the D ekany model (22), present such a network. The model proposed by D ekany *et al.* may be correct for their more highly oxidized compound, because that structural model seems to call for a considerably higher level of oxidization to complete the modification of an sp^2 network into a network of linked cyclohexanes. Further studies would be needed to define all of the structural details of the system.

Chemically modified graphenes that will be of importance in a variety of new materials can now be ^{13}C -labeled and more effectively studied by SSNMR. High-quality ^{13}C -labeled graphite should find use for fundamental property measurements, including of ^{13}C -labeled graphene.

References and Notes

1. B. C. Brodie, *Annales des Chimie et des Physique* **59**, 466 (1860).
2. S. Stankovich *et al.*, *Carbon* **45**, 1558 (2007).
3. S. Stankovich *et al.*, *J. Mater. Chem.* **16**, 155 (2006).
4. M. J. McAllister *et al.*, *Chem. Mater.* **19**, 4396 (2007).
5. D. A. Dikin *et al.*, *Nature* **448**, 457 (2007).
6. S. Stankovich *et al.*, *Nature* **442**, 282 (2006).
7. S. Stankovich, R. D. Piner, S. T. Nguyen, R. S. Ruoff, *Carbon* **44**, 3342 (2006).
8. S. Watcharotone *et al.*, *Nano Lett.* **7**, 1888 (2007).
9. H. H. Angermann, G. Horz, *Appl. Surf. Sci.* **70-71**, 163 (1993).
10. R. Anton, *J. Mater. Res.* **20**, 1837 (2005).
11. A. Barbangolo, R. Sangiorgi, *Mater. Sci. Eng. A* **156**, 217 (1992).

12. F. Bonnet, F. Ropital, Y. Berthier, P. Marcus, *Mater. Corrosion Werkst. Korros.* **54**, 870 (2003).
13. D. V. Fedoseev, S. P. Nvukov, B. V. Derjaguin, *Carbon* **17**, 453 (1979).
14. D. Fujita, T. Homma, *Surf. Interface Anal.* **19**, 430 (1992).
15. D. Fujita, K. Yoshihara, *J. Vac. Sci. Technol. A* **12**, 2134 (1994).
16. C. Klink, I. Stensgaard, F. Besenbacher, E. Laegsgaard, *Surf. Sci.* **342**, 250 (1995).
17. A. N. Obratsov, E. A. Obratsova, A. V. Tyurnina, A. A. Zolotukhin, *Carbon* **45**, 2017 (2007).
18. H. Oudghiri-Hassani, S. Rakass, N. Abatzoglou, P. Rowntree, *J. Power Sources* **171**, 850 (2007).
19. R. Sinclair, T. Itoh, R. Chin, *Microsc. Microanal.* **8**, 288 (2002).
20. M. Yudasaka, R. Kikuchi, Y. Ohki, S. Yoshimura, *J. Vac. Sci. Technol. A* **16**, 2463 (1998).
21. Materials and methods are available as supporting material on Science Online.
22. T. Szabo *et al.*, *Chem. Mater.* **18**, 2740 (2006).
23. A. Lerf, H. Y. He, M. Forster, J. Klinowski, *J. Phys. Chem. B* **102**, 4477 (1998).
24. Y. Ishii, *J. Chem. Phys.* **114**, 8473 (2001).
25. ^{13}C was provided through a research grant from Cambridge Isotopes Laboratories, Inc. We (R.S.R.) wish to acknowledge The University of Texas for startup funds and for partial support by the *Defense Advanced Research Projects Agency* Center on Nanoscale Science and Technology for Integrated Micro/NanoElectromechanical Transducers (HR0011-06-1-0048). The WiTec Micro-Raman instrument was acquired by an Air Force Office of Scientific Research, Defense University Research Instrumentation Program grant. Y.I. appreciates support from the Dreyfus Foundation Teacher-Scholar Award program and the NSF CAREER program (CHE 449952). S.J.A. was financially supported by the Korea Science and Engineering Foundation under the National Creative Research Initiative Project (R16-2004-004-01001-0) of the Ministry of Science and Technology, Korea. J. Goodenough and A. Ruoff commented on an early version of this manuscript.

Supporting Online Material

www.sciencemag.org/cgi/content/full/321/5897/1815/DC1
Materials and Methods
Figs. S1 to S5
References

26 June 2008; accepted 15 August 2008
10.1126/science.1162369

Linear Response Breakdown in Solvation Dynamics Induced by Atomic Electron-Transfer Reactions

Arthur E. Bragg, Molly C. Cavanagh, Benjamin J. Schwartz*

The linear response (LR) approximation, which predicts identical relaxation rates from all nonequilibrium initial conditions that relax to the same equilibrium state, underlies dominant models of how solvation influences chemical reactivity. We experimentally tested the validity of LR for the solvation that accompanies partial electron transfer to and from a monatomic solute in solution. We photochemically prepared the species with stoichiometry Na^0 in liquid tetrahydrofuran by both adding an electron to Na^+ and removing an electron from Na^- . Because atoms lack nuclear degrees of freedom, ultrafast changes in the Na^0 absorption spectrum reflected the solvation that began from our two initial nonequilibrium conditions. We found that the solvation of Na^0 occurs more rapidly from Na^+ than Na^- , constituting a breakdown of LR. This indicates that Marcus theory would fail to describe electron-transfer processes for this and related chemical systems.

Solvent-solute interactions play an integral role in solution-phase chemical reactivity and particularly in electron-transfer (ET) reactions (1), in which solvation dynamics—the

response of the solvent to changes in solute size and/or electronic charge distribution (2)—help drive the motion of charge from donor to acceptor. Current theoretical understanding of how

solvation dynamics influence chemical reactivity [for example, through the Marcus theory of ET (*I*)] is based largely on the idea of linear response (LR) (3–6). If the Hamiltonian governing solute-solvent interactions is assumed to change linearly with respect to a perturbation that moves the system out of equilibrium, then the relaxation of the perturbed nonequilibrated state should be identical to the regression of the spontaneous fluctuations of the system at equilibrium; this assumption is commonly called the LR approximation (3). In this work, we performed an experimental test of LR in which we investigated the solvation dynamics associated with elementary steps that play a role in many common chemical transformations, specifically the spontaneous partial transfer of an electron to and from an atomic solute in solution. We demonstrate that the LR approximation fails to underlie the solvation processes associated with this particular atomic ET reaction, leading us to predict that LR may break down more broadly in solution-phase chemical dynamics than previously appreciated.

A convenient way to characterize the evolution of solute-solvent interactions is to use the framework of time correlation functions (TCFs). At equilibrium, the evolution of solvent-solute interactions can be quantified by Eq. 1

$$C(t) = \frac{\langle \delta E(t) \delta E(0) \rangle}{\langle \delta E(0)^2 \rangle} \quad (1)$$

which autocorrelates the fluctuations of the solute-solvent interaction energy E about its average value, $\delta E(t) = E(t) - \langle E \rangle$; the angled brackets represent equilibrium ensemble averages. This TCF can be viewed as describing the time scale of the intrinsic fluctuations of an equilibrium solvent-solute system: if we artificially prepared a specific solvent-solute configuration that could be reached via thermal fluctuations at equilibrium, then $C(t)$ would reflect the time dependence of the subsequent relaxation away from this configuration. Within the limit of LR, the nonequilibrium relaxation of the solvent-solute interaction energy after perturbation of the system from equilibrium, $S(t)$, should match the TCF of the system at equilibrium (3, 7, 8)

$$S(t) = \frac{\overline{E}(t) - \overline{E}(\infty)}{\overline{E}(0) - \overline{E}(\infty)} \approx C(t) \quad (2)$$

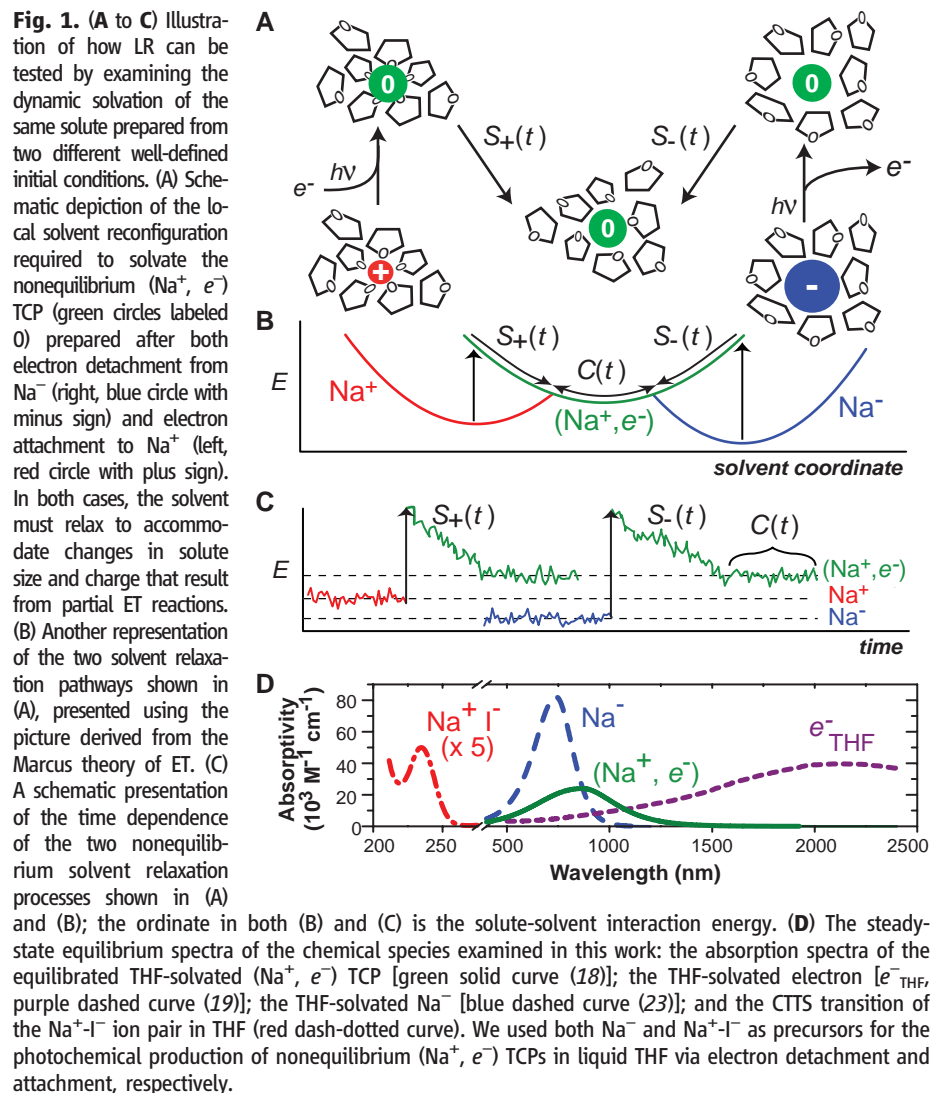
where the overbars indicate nonequilibrium ensemble averages. Although the LR approximation (Eq. 2) can be derived from statistical mechanical perturbation theory (and thus is applicable when the perturbation to a system is near thermal energies [Boltzmann's constant

times the temperature ($\sim k_B T$) (3)), it has recently been shown that LR arises whenever the fluctuations of a system are Gaussian, regardless of the magnitude of the deviation from equilibrium (5, 7, 8). It is these Gaussian statistics, in turn, that give rise to the familiar parabolic potentials along the generalized solvent coordinate that lie at the foundation of the Marcus theory of ET (*I*). Thus, when valid, the LR approximation provides a useful means of estimating and interpreting theoretically the time-dependent relaxation that follows the preparation of many (*I*, 3–5, 8), but not all (6, 7, 9), highly perturbed solvent-solute configurations.

How can we test the validity of LR experimentally, particularly for the solvation dynamics tied to chemical reactivity? To test LR directly, we must not only track the dynamics of quantity associated with the time-evolving solute-solvent interaction as the system relaxes from a well-defined nonequilibrium configuration [$S(t)$], but also measure the solvent-solute fluctuations at equilibrium [$C(t)$]. Unfortunately, the equilibrium TCF is difficult to access, although a recently developed approach that mea-

sures the difference in solvent spectral density after the photoexcitation of a probe solute shows great promise toward making this direct comparison (*10*). Here, we describe an alternative approach to assess the LR approximation: We compare the relaxation dynamics that begin from two different well-defined nonequilibrium configurations but end in the same final equilibrium state. If LR holds, then the time dependence of the solvent-solute relaxation from both nonequilibrium states should be identical to the equilibrium TCF. If the two nonequilibrium configurations relax on different time scales, as we discuss below, then the LR prediction must fail to describe one or both of the relaxation pathways.

Although our approach should apply to any solute-solvent system, we have chosen to survey the relaxation of atoms in solution because these solutes lack internal nuclear degrees of freedom. Thus, unlike the large molecular chromophores that are typically used as solvation probes, the atomic relaxation dynamics that we observe directly reflect the motions of the surrounding solvent and are unobscured by competing intramolecular processes (*11*). Specifically, we ex-



Department of Chemistry and Biochemistry, University of California, Los Angeles Los Angeles, CA 90095-1569, USA.

*To whom correspondence should be addressed. E-mail: schwartz@chem.ucla.edu

amined the nonequilibrium relaxation of neutral atomic sodium (Na^0) in liquid tetrahydrofuran (THF) that was prepared both by photoinduced ET to sodium cations (Na^+) and by electron photodetachment from sodium anions (Na^- , or sodide). Figure 1A schematically illustrates the solvent reconfiguration that occurs after each of these photochemical preparations; Fig. 1B presents this same relaxation in terms of the picture derived from the Marcus theory of ET, in which the relaxation of the solvent-solute interaction energy, E , is expressed as a function of a collective solvent coordinate; and Fig. 1C illustrates the time-dependent solute-solvent interaction energy as would be typically examined in a molecular dynamics (MD) simulation. The red and blue curves in Fig. 1C reflect fluctuations of the ion-solvent interactions about their equilibrium average values before each photochemical process. If we promptly add or remove an electron to or from one of the initially equilibrated ions through photoinduced ET (vertical black arrows in Fig. 1, A to C), the solvent interaction energy associated with the newly created neutral solute will be outside the range of the equilibrium fluctuations [green curves labeled $C(t)$ in Fig. 1, B and C], because the initial solvent structure is equi-

brated for an ion and thus poorly accommodates the neutral Na. The nearby solvent molecules will then relax by both translating to accommodate the change in solute size and rotating so that the solvent dipoles become favorably oriented for the neutral Na. We label the nonequilibrium relaxation of the neutral Na that begins with the initial configuration characteristic of the Na anion " $S_-(t)$ " (right side of Fig. 1, A to C), and we label the relaxation that begins from the initial configuration associated with the Na cation " $S_+(t)$ " (left side of Fig. 1, A to C). If LR holds, then we expect $S_+(t) = S_-(t)$ because both should be equal to $C(t)$.

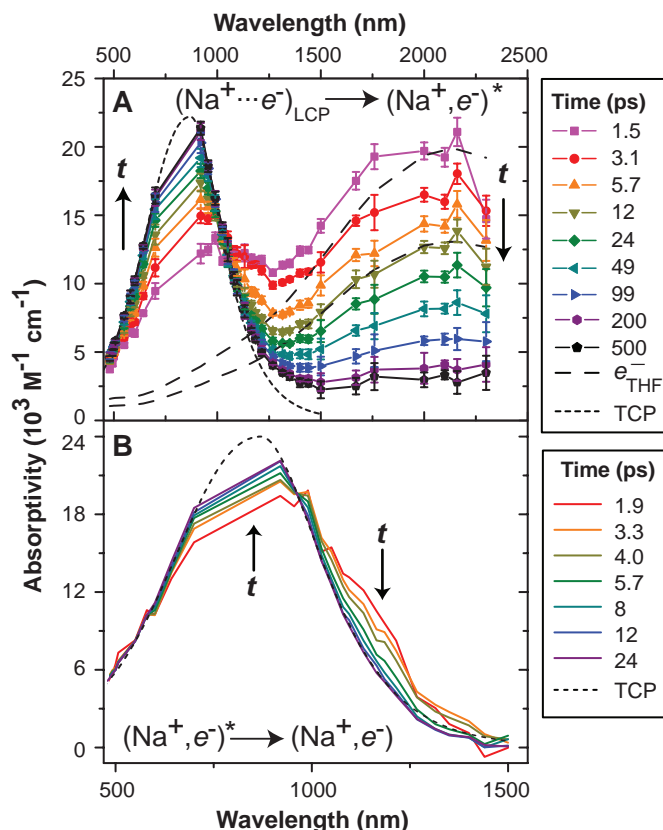
Atomic Na in THF is a convenient system for testing the LR approximation through this approach for several reasons. The precursors we used to create neutral Na photochemically (Na^- and the $\text{Na}^+\text{-I}^-$ ion pair) are stable in liquid THF. In addition, the solvent structure and the nature of the delocalized solvent-supported electronic states of liquid THF (12, 13) allow us to rapidly shuttle electrons to and from these ion precursors via photoinduced ET (14, 15). Finally, the spectrum of atomic Na in THF is highly sensitive to the nature of the local solvent environment (16) and spans visible and near-infrared wavelengths (Fig. 1D, green solid curve),

so we can easily track the solvation dynamics that follow each photochemical preparation, using transient absorption spectroscopy.

The extraordinary sensitivity of the Na atom's absorption spectrum to the local solvent environment arises from the chemical nature of Na in THF: Rather than a solvated atom, the equilibrated neutral Na solute in THF is better thought of as a (Na^+, e^-) tight-contact pair (TCP), in which the electron has substantial interactions with the solvent as well as a partial-valence interaction with the Na cation core (16, 17). The steady-state absorption spectrum of the (Na^+, e^-) TCP peaks at 870 nm [Fig. 1D, green solid curve (18)], a wavelength that lies between the narrow gas-phase Na D line (peaking at 590 nm) and the broad absorption of the THF-solvated electron, e^-_{THF} [Fig. 1D, purple dotted curve, peaking at 2160 nm (19)], reflecting the fact that the chemical nature of this solute lies between the extremes of pure cation-electron and solvent-electron interactions. As a result, the TCP is formed from either a solvent-separated $\text{Na}^+ + e^-_{\text{THF}}$ pair or a weakly solvated, gas-phase-like Na^0 atom by partial transfer of an electron toward or away from the Na^+ core, respectively



Fig. 2. Ultrafast transient absorption dynamics after the 263-nm CTTS excitation of $\text{Na}^+\text{-I}^-$ in liquid THF. (A) Spectral reconstruction (SOM text) showing the dynamics of Na^+e^- attachment to form the (Na^+, e^-) TCP; the symbols represent the data, which are connected with colored lines to guide the eye (the large linear region near 800 nm results from difficulty in probing near the laser fundamental with our transient absorption setup; error bars represent 95% confidence limits of measurements). The fact that the early-time data do not match the equilibrium spectrum of e^-_{THF} (shown as the long-dashed black curves that have been scaled for ease of comparison to the data at 1.5 and 12 ps) near ~ 1700 nm indicates that some of the CTTS-generated electrons rapidly attach to Na^+ to form Na cation-electron



LCPs. The short-dashed black curve shows the equilibrium (Na^+, e^-) TCP spectrum for reference. (B) Spectral dynamics associated with the (Na^+, e^-) TCP created after electron attachment [colored lines, as in (A)]; the spectrum of this species has been isolated by subtracting the contributions of e^-_{THF} and $(\text{Na}^+ \cdots e^-)_{\text{LCP}}$ (SOM text). The data show that after the LCP \rightarrow TCP partial ET reaction, dynamic solvation results in a spectral blue shift of the nonequilibrium TCP absorption that occurs on a ~ 5 -ps time scale. Different wavelength scales are used in (A) and (B).

In our experiments, we used two different photoinduced ET processes (Fig. 1, A to C) to create the species on both the left and right of Eq. 3 and then track the solvation dynamics associated with the spontaneous partial ET reactions that generate (Na^+, e^-) as a result of the subsequent solvent-solute relaxation.

The THF-solvated (Na^+, e^-) TCP can be generated readily from its constituent parts, Na^+ and e^- (left side of Eq. 3) (18), but under most conditions it is challenging to measure the dynamic solvation of a solute produced through electron attachment, because the rate of attachment is generally limited by the mutual diffusion of the reactants. However, by taking advantage of the relatively strong ion-pair interactions that exist in weakly polar solvents such as THF, we can locate an electron-donating chromophore (here, iodide) close to the Na cation and thus photo-initiate prompt electron attachment. In previous work, we showed that electrons generated through charge-transfer-to-solvent (CTTS) excitation of counterion-free iodide in THF were ejected ~ 6 nm away from the iodine core (20), but that the presence of nearby Na^+ collapses the CTTS-electron ejection distribution within ~ 2 nm of the cation, so that $>50\%$ of the electrons attach to Na^+ to form (Na^+, e^-) TCPs within 2 ps (21). Consequently, the $\text{Na}^+\text{-I}^-$ ion pair in THF provides an ideal precursor to create our (Na^+, e^-) TCP solvation probe from its constituent parts via excitation of the $\text{Na}^+\text{-I}^-$ CTTS band (Fig. 1D, red dot-dashed curve) and to subsequently probe in detail the ultrafast solvation dynamics associated with electron attachment, $S_+(t)$.

Figure 2A presents the temporal evolution of the transient absorption that follows the 263-nm CTTS excitation of 20-mM NaI in THF [see the supporting online material (SOM) text for details (22)]. The data show that CTTS excitation rapidly induces an absorption in the 1200- to 2300-nm spectral region. This absorption then decays over the course of 200 to 300 ps concurrently with the appearance of a new absorption band in the 480- to 900-nm region. The absorption dynamics at intermediate wavelengths (900 to 1200 nm) evolve with more complexity, although a quasi-isosbestic point appears near 1130 nm. To first order, these spectral dynamics reflect the disappearance of CTTS-generated THF-solvated electrons (e^-_{THF}) as they diffusively attach to nearby Na^+ in solution to form the (Na^+, e^-) TCP (21).

A closer examination of Fig. 2A, however, reveals that the spectrum measured between 1200 and 2300 nm immediately after CTTS excitation of NaI (at 1.5 ps, pink trace) does not match that of the equilibrated THF-solvated electron (scaled and plotted as long-dashed curves). We have observed a similar spectrum (that is, slightly blue-shifted relative to the spectrum of e^-_{THF}) after the CTTS excitation of tetrabutylammonium iodide ($t\text{-BA}^+\text{-I}^-$) in THF (21), and we determined that the weak ion-pair interactions between I^- and $t\text{-BA}^+$ promote the forma-

tion of a loose cation-electron contact pair (LCP). The LCP is characterized by a weak Coulombic cation-electron attraction (not the stronger partial valence interactions that define the TCP), and its spectrum can be thought of as arising from a Stark shift of the e^-_{THF} absorption induced by the presence of the nearby cation. For the $\text{Na}^+\text{-I}^-$ system studied here, the spectrum between 1200 and 2300 nm (Fig. 2A) rapidly decays in intensity over the initial few picoseconds as TCPs are formed, with the remaining feature matching the shape of the e^-_{THF} spectrum by ~ 12 ps (light green trace). Thus, the data in Fig. 2A demonstrate the transient formation of a sizeable $\text{Na}^+\text{-}e^-$ LCP population after CTTS excitation of $\text{Na}^+\text{-I}^-$ in THF (21, 22)

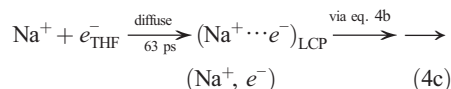
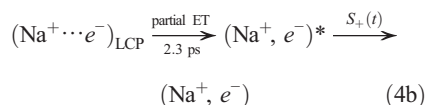
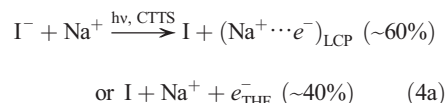
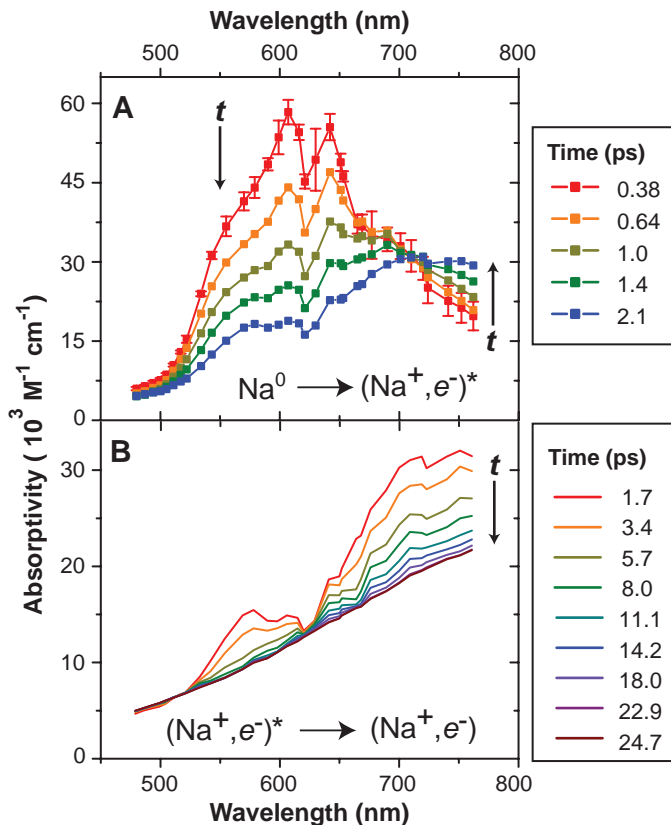


Fig. 3. Spectrally reconstructed ultrafast transient absorption dynamics of the neutral Na species created after 395-nm CTTS excitation of Na^- in liquid THF [(16) and SOM text (22)]. (A) Spectral dynamics (squares connected by colored lines to guide the eye; error bars represent 95% confidence limits of measurements) associated with the chemical conversion of a weakly solvated Na atom, characterized by the split and broadened Na D-line transition near 600 nm (0.38 ps), to become the THF-solvated (Na^+, e^-) TCP; the isosbestic point near 720 nm indicates that Na^0 and (Na^+, e^-) TCPs are chemically distinct species that interconvert via a spontaneous partial ET reaction. (B) Spectral dynamics associated with the (Na^+, e^-) TCP after electron detachment (colored lines); the



spectral dynamics of this species have been isolated by subtracting the contribution from Na^0 and have been normalized to remove contributions from changes in TCP population [(16) and SOM text]. The data demonstrate that after the $\text{Na}^0 \rightarrow (\text{Na}^+, e^-)$ partial ET reaction, dynamic solvation results in a substantial red shift of the nonequilibrium TCP absorption that occurs on a ~ 10 -ps time scale.

$(\text{Na}^+, e^-)^*$ denotes a nonequilibrated TCP solute, and I is a spectator in Eqs. 4b and 4c [(SOM text) (22)]. As a result, CTTS excitation of NaI allows us to rapidly create a population of LCPs, which then spontaneously convert to a nonequilibrium $(\text{Na}^+, e^-)^*$ TCP population via partial ET to Na^+ .

We can isolate the spectral evolution associated with TCP solvation by subtracting the spectral contributions from the LCP and e^-_{THF} [the latter formed in $\sim 40\%$ yield after CTTS ejection from iodide to locations far from a Na^+ cation (Eq. 4a)], and by normalizing for TCP population kinetics, as plotted in Fig. 2B [(SOM text) (22)]. Although the first ~ 2 ps of the TCP spectral dynamics are obscured by the LCP \rightarrow TCP interconversion process as well as by experimental resolution effects (21), the data clearly show that the initially produced $(\text{Na}^+, e^-)^*$ species (at 1.9 ps) has a spectrum that is red-shifted and slightly broadened relative to the equilibrium absorption (black dashed curve). As the solvent relaxes, the transient spectrum of the TCP blue-shifts and narrows on a ~ 5 -ps time scale, with solvation complete by 10 ps. Because the TCP solvation dynamics we measured may be rate-limited by the LCP \rightarrow TCP reaction process (the first step of Eq. 4b), this ~ 5 -ps time scale represents an upper limit for the decay of $S_+(t)$.

To examine the nonequilibrium solvation of the same (Na^+, e^-) TCP solute from a different initial solvent-solute configuration (Fig. 1, A to C, right panels), we also created the TCP in a solvent environment that initially accommodates its corresponding anion, Na^- . Like I^- , Na^- in liquid THF has a strong CTTS transition [Fig. 1D, blue dashed curve (23)], photoexcitation of which leads to subpicosecond electron ejection and

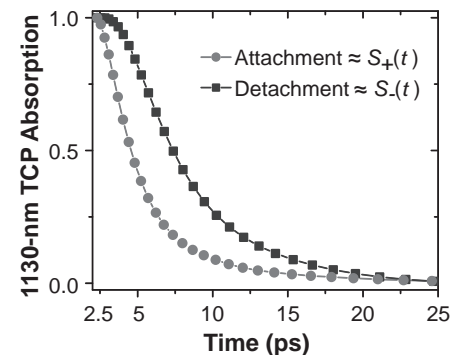
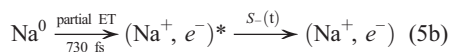
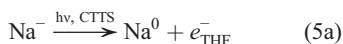


Fig. 4. Ultrafast spectral dynamics, probed at 1130 nm, of the (Na^+, e^-) TCP created after both electron attachment via 263-nm CTTS excitation of $\text{Na}^+\text{-I}^-$ [circles, $S_+(t)$] and electron detachment via 395-nm CTTS excitation of Na^- [squares, $S_-(t)$]. The two spectral transients have been normalized at 2 ps and the detachment data have been inverted for ease of comparison. To the extent that probing at a single wavelength characterizes the entire solvent response (26), the data show that solvation of the nonequilibrium TCP occurs roughly twice as fast after electron attachment than after electron detachment ($1/e$ time scales of 3.9 and 7.5 ps, respectively), thus demonstrating a breakdown of LR.

leaves behind a neutral atomic Na core. Because of the cavities that are inherent in the structure of liquid THF (12, 13), the distance to which the CTTS-generated electrons are ejected from the neutral Na core increases with increasing excitation energy (24). Thus, by exciting the Na⁻ CTTS transition at 395 nm, we are able to move the CTTS-generated electron far from the Na⁰ core, so that the spectral dynamics we measure for Na⁰ are negligibly affected by the proximity of (or possible recombination with) the CTTS-ejected electron (16). The spectral dynamics associated with the Na⁰ product generated via 395-nm excitation of the Na⁻ CTTS band, corrected for the modest Na⁰-e⁻_{THF} recombination that does take place, are shown in Fig. 3 (16, 22).

The spectrum of the nascent neutral Na atom measured immediately after electron photodetachment from Na⁻ (at 0.38 ps) exhibits a broad, intense absorption band that peaks between 600 and 650 nm. We (16) and others (25) have assigned this feature to the sodium D-line transition, albeit broadened and split by the asymmetry of the surrounding solvent cavity. The similarity in the position of this band to that measured in the gas phase reflects the weak interaction of the nascent neutral atom with the surrounding solvent; this is expected because the initial solvent structure had accommodated equilibrated Na⁻, which is much larger than the neutral Na atom (Fig. 1A, right) (16). Figure 3A further reveals that this initially produced D-line absorption feature decays substantially over the next ~2 ps and that the decay is accompanied by a concomitant increase in spectral intensity at longer wavelengths (>700 nm); a well-defined isosbestic point at ~720 nm indicates that these spectral changes result from a kinetic interconversion between two chemically distinct species. Careful analysis of this spectral progression reveals that the neutral Na solute starts from a state in which the 3s valence electron is bound almost exclusively by the Na⁺ core but then undergoes a spontaneous partial ET reaction on a ~730-fs time scale to produce a nonequilibrated (Na⁺, e⁻)* TCP in which the electron is subject to substantial interactions with the solvent (16)



After this partial ET from the nascent neutral atom (which was produced via photoinduced CTTS detachment from Na⁻), (Na⁺, e⁻)* relaxes with the surrounding solvent to reach equilibrium, *S*₋(*t*).

Figure 3B highlights the spectral evolution of the TCP during the *S*₋(*t*) relaxation, which has been isolated by removing contributions from the Na⁰ absorption at 600 nm and normalized for its time-dependent population kinetics (16, 22). The solvation induced evolution of the (Na⁺, e⁻)

spectrum occurs more slowly than the partial ET reaction that forms this species from Na⁰. Figure 3B shows that the time-dependent TCP spectrum red shifts (and broadens to maintain a constant oscillator strength) as it relaxes to equilibrium. The data show that this dynamic solvation process takes place on a ~10-ps time scale and that the *S*₋(*t*) relaxation is not complete for at least 20 to 25 ps.

One way to approximately quantify the *S*₊(*t*) and *S*₋(*t*) TCFs inherent to the data in Figs. 2B and 3B is to compare the dynamics at a single wavelength (26). Thus, in Fig. 4, we compare the time-dependent TCP spectral dynamics at 1130 nm for both solvation processes. We chose this wavelength for two reasons. First, 1130 nm lies near the isosbestic point for the TCP and LCP/e⁻_{THF} absorption bands; thus, for the photoinduced electron-attachment pathway, this wavelength probes primarily TCP solvation and not population dynamics, guaranteeing that the kinetic model we used to deconstruct our data does not influence the *S*₋(*t*) solvation response we derive at this wavelength [(SOM text) (22)]. Second, the long-time TCP solvation after electron photodetachment is observed most cleanly at this wavelength, because there is no interference from Na⁻ bleach and the e⁻_{THF} absorption contribution can be removed readily (16). To directly compare the 1130-nm spectral dynamics from the two pathways, we have inverted the *S*₋(*t*) response from the photodetachment pathway, because the TCP spectral red shift results in a delayed rise (rather than a decay) at this wavelength (16). We also have normalized the 1130-nm spectral transients at 2 ps in order to focus on the long-time solvation dynamics and to exclude contributions from the faster ET interconversion kinetics observed along both relaxation pathways. Figure 4 indeed illustrates that, as estimated by the 1130-nm spectral dynamics, *S*₊(*t*) decays roughly twice as fast as *S*₋(*t*) (1/*e* time scales of 3.9- and 7.5-ps, respectively). Because we know that the *S*₊(*t*) response is partly rate-limited by the LCP → TCP conversion process, whereas the *S*₋(*t*) response occurs more slowly than the Na⁰ → (Na⁺, e⁻) reaction time scale, this difference in the two responses represents a lower limit.

Together, Figs. 2B, 3B, and 4 prove that LR does not apply for the solvation dynamics that accompany the creation of the (Na⁺, e⁻) TCP through the two different partial ET reactions. The *S*₋(*t*) solvation response that follows the creation of the TCP via partial ET from a LCP [which was created via electron photoattachment (Eq. 4)] starts from a solvent configuration that was optimized to accommodate the small Na⁺, prompting a blue shift of the TCP spectrum that is complete within ~10 ps; this time scale is similar to the solvent relaxation measured after the excitation of a dye molecule in liquid THF (27). In contrast, the *S*₋(*t*) solvation response that follows the creation of the TCP via partial ET from Na⁰ (Eq. 5) starts from a solvent configuration

that was optimized to accommodate the large Na⁻ anion, prompting a red shift of the TCP spectrum that is not complete for 20 to 25 ps. This large difference in time scale in the solvation dynamics of the same species approaching equilibrium from two different initial configurations is a clear indication that the LR approximation, which predicts identical *S*₊(*t*) and *S*₋(*t*) responses, does not describe the solvation dynamics that follow these simple partial electron-transfer reactions.

Why should we observe this breakdown of LR? Guided by results of MD simulations that have demonstrated a failure of LR similar to what we observed here (6), we believe that the changes in solute size involved in these partial charge-transfer reactions help promote the breakdown of LR. These simulations revealed that when the solute size decreases (as occurs upon the removal of an electron), the rate of the solvent response is essentially limited by the translational diffusion of first-shell solvent molecules into the void space left behind after the solute shrinks. Thus, we expect LR to break down in this case both because the initial solvent configuration about the smaller solute is never explored through equilibrium fluctuations and because the corresponding diffusional solvent motions that relax this configuration are slower than those at equilibrium. In contrast, the simulations also have shown that the solvent response that accompanies a solute size increase (as occurs upon the addition of an electron) is driven rapidly by strong, short-ranged repulsive interactions between the enlarged solute and the first-shell solvent molecules. The fact that *S*₋(*t*) is substantially slower than *S*₊(*t*) strongly suggests that the relative changes in size of the initial Na⁰ and LCP as they become the TCP are primarily responsible for the breakdown of LR that we observed in our experiments.

To what extent do the processes we have studied reflect the solute-solvent relaxation in more common chemical transformations? Is the breakdown of LR we observed in this model system the rule, and not an exception, for the nonequilibrium solvation that occurs in the course of typical chemical processes? In addition to our observations, a breakdown of LR has recently been observed to follow the photodissociation of the ICN molecule in ethanol (28), which produces a CN fragment whose excited rotational motion is only slowly quenched by interactions with the surrounding solvent. This behavior demonstrates an anticipated failure of LR in scenarios in which a chemical process partitions substantial internal energy (many *k*_B*T*) into a product fragment (7, 28). Even though the photochemical preparation in our experiments involves photons with energies of hundreds of *k*_B*T*, most of this energy is used to detach an electron from either Na⁻ or I⁻ and move it through liquid THF; the bulk of this energy is not partitioned directly to the TCP product. Moreover, our experiments measure the TCP solvation only after spontaneous partial ET

reactions (Eqs. 3 to 5). Thus, although we may anticipate that the solvation dynamics measured involve substantial changes in the local solvation structure due to the solute size change, we expect that the energies associated with $(\text{Na}^+, e^-)^*$ formation are not chemically extreme and are representative of those associated with common solution-phase reactions.

This clear breakdown of LR implies that the solvent fluctuations coupled to the (Na^+, e^-) TCP are not Gaussian, and thus that the potential surfaces associated with these ET processes are highly nonparabolic. As a result, the Marcus theory of ET would poorly describe these ET processes. We anticipate that this could be an important consideration in many similar outer-sphere ET reactions, where substantial rearrangement of the local solvent structure could induce a similar LR breakdown. It is also important to note that the LR approximation is built on the idea that the same solvent-solute motions that underlie equilibrium fluctuations are also responsible for the nonequilibrium solvation dynamics (3). Although we observed a clear difference in the time dependence of two solvation pathways that reflects a breakdown of LR, observing an identical time dependence would not have guaranteed that the LR holds. This is because even when the specific molecular motions responsible for relaxing a nonequilibrium perturbation differ considerably from the solvent fluctuations active at equilibrium, LR may appear to be valid if the relevant nonequilibrium and equilibrium solvent

motions happen to occur on similar time scales; what we have termed a hidden breakdown of LR (29, 30). Overall, these findings demonstrate that an accurate assessment of solvation dynamics—and, by extension, our understanding of solution-phase chemical reactivity—must be considered directly at the molecular level in order to determine correctly how best to understand the solvent relaxation resulting from a given nonequilibrium perturbation.

References and Notes

- R. A. Marcus, N. Sutin, *Biochim. Biophys. Acta* **811**, 265 (1985).
- M. Maroncelli, *J. Mol. Liq.* **57**, 1 (1993).
- D. Chandler, *Introduction to Modern Statistical Mechanics* (Oxford Univ. Press, New York, 1987).
- R. M. Strat, M. Maroncelli, *J. Phys. Chem.* **100**, 12981 (1996).
- P. L. Geissler, D. Chandler, *J. Chem. Phys.* **113**, 9759 (2000).
- D. Aherne, V. Tran, B. J. Schwartz, *J. Phys. Chem. B* **104**, 5382 (2000).
- G. Tao, R. M. Strat, *J. Chem. Phys.* **125**, 114501 (2006).
- B. B. Laird, W. H. Thompson, *J. Chem. Phys.* **126**, 211104 (2007).
- T. Fonseca, B. M. Ladanyi, *J. Phys. Chem.* **95**, 2116 (1991).
- D. F. Underwood, D. A. Blank, *J. Phys. Chem. A* **109**, 3295 (2005).
- D. S. Larsen, K. Ohta, Q. H. Xu, M. Cyrier, G. R. Fleming, *J. Chem. Phys.* **114**, 8008 (2001).
- M. J. Bedard-Hearn, R. E. Larsen, B. J. Schwartz, *J. Chem. Phys.* **122**, 134506 (2005).
- D. T. Bowron, J. L. Finney, A. K. Soper, *J. Am. Chem. Soc.* **128**, 5119 (2006).
- M. J. Bedard-Hearn, R. E. Larsen, B. J. Schwartz, *J. Chem. Phys.* **125**, 194509 (2006).
- I. B. Martini, E. R. Barthel, B. J. Schwartz, *Science* **293**, 462 (2001).

- M. C. Cavanagh, R. E. Larsen, B. J. Schwartz, *J. Phys. Chem. A* **111**, 5144 (2007).
- R. Catterall, J. Slater, M. C. R. Symons, *J. Chem. Phys.* **52**, 1003 (1970).
- B. Bockrath, L. M. Dorfman, *J. Phys. Chem.* **77**, 1002 (1973).
- F.-Y. Jou, G. R. Freeman, *Can. J. Chem.* **57**, 591 (1979).
- A. E. Bragg, B. J. Schwartz, *J. Phys. Chem. B* **112**, 483 (2008).
- A. E. Bragg, B. J. Schwartz, *J. Phys. Chem. A* **112**, 3530 (2008).
- Methods are detailed in supporting material available on Science Online.
- M. T. Lok, J. L. Dye, F. J. Tehan, *J. Phys. Chem.* **76**, 2975 (1972).
- E. R. Barthel, B. J. Schwartz, *Chem. Phys. Lett.* **375**, 435 (2003).
- O. Shoshana, J. L. Pérez Lustres, N. P. Ernstring, S. Ruhman, *Phys. Chem. Chem. Phys.* **8**, 2599 (2006).
- V. Nagarajan, A. M. Brearley, T.-J. Kang, P. F. Barbara, *J. Chem. Phys.* **86**, 3183 (1987).
- L. Reynolds, J. A. Gardecki, S. J. V. Frankland, M. L. Horng, M. Maroncelli, *J. Phys. Chem.* **100**, 10337 (1996).
- A. C. Moskun, A. E. Jalaubekov, S. E. Bradforth, G. Tao, R. M. Strat, *Science* **311**, 1907 (2006).
- M. J. Bedard-Hearn, R. E. Larsen, B. J. Schwartz, *J. Phys. Chem. A* **107**, 4773 (2003).
- M. J. Bedard-Hearn, R. E. Larsen, B. J. Schwartz, *Phys. Rev. Lett.* **97**, 130403 (2006).
- This research was funded by NSF under grant number CHE-0603766. The authors thank R. E. Larsen for useful discussions and a critical reading of the manuscript.

Supporting Online Material

www.sciencemag.org/cgi/content/full/321/5897/1817/DC1
SOM Text
Figs. S1 to S4
References

9 June 2008; accepted 18 August 2008
10.1126/science.1161511

Mars' Paleomagnetic Field as the Result of a Single-Hemisphere Dynamo

Sabine Stanley,^{1*} Linda Elkins-Tanton,² Maria T. Zuber,² E. Marc Parmentier³

Mars' crustal magnetic field was most likely generated by dynamo action in the planet's early history. Unexplained characteristics of the field include its strength, concentration in the southern hemisphere, and lack of correlation with any surface features except for the hemispheric crustal dichotomy. We used numerical dynamo modeling to demonstrate that the mechanisms proposed to explain crustal dichotomy formation can result in a single-hemisphere dynamo. This dynamo produces strong magnetic fields in only the southern hemisphere. This magnetic field morphology can explain why Mars' crustal magnetic field intensities are substantially stronger in the southern hemisphere without relying on any postdynamo mechanisms.

The Mars Global Surveyor mission showed that Mars possesses remanent crustal magnetic fields from a dynamo that was operational for a short time in Mars' early history (1). Remanent crustal magnetism is observed in early Noachian (>3.9 billion years old) crust in both

the northern and southern hemispheres, except for much of the Tharsis volcanic province and the large impact basins Hellas and Argyre in the southern hemisphere, and Isidis and Utopia in the northern hemisphere. There is a conspicuous difference in the magnetic field intensities in the two hemispheres: The northern hemisphere contains only weak magnetic fields, whereas the southern hemisphere contains both strong and weak fields (2).

The timing of the dynamo is constrained by the observations that the floors of the large impact basins formed during the Late Heavy Bombardment [~3.9 billion years ago (Ga)] are not

magnetized (1) and that the ancient Martian meteorite ALH84001 contains a remanent magnetic field dated earlier than 3.9 Ga (3). Most likely, the dynamo was active sometime between core formation (~4.5 Ga) and the Late Heavy Bombardment. The driving force for the dynamo, the intensity and morphology of the generated field, and the cause of the dynamo's demise are not well understood.

Another ancient Martian crustal feature is the hemispheric dichotomy. The northern and southern hemispheres have similar-aged crusts (4) but different topographies, thicknesses, and sediment covers (5). The northern hemisphere crust is low, thin, and covered with volcanic flows and sediments, whereas the southern hemisphere crust is high, thick, and largely devoid of sedimentary or volcanic resurfacing. Cratering evidence and the dichotomy's long wavelength suggest that the dichotomy is an ancient feature, directly related to crustal formation sometime between 4.5 and 3.9 Ga (6, 7).

Because the crustal magnetic field and the dichotomy are similar in age, it is possible that their formation processes are related. Several endogenic mechanisms could explain both dichotomy formation and a concurrent dynamo sometime between 4.5 and 3.9 Ga. A hemispheric-scale (degree-1) pattern of mantle circulation resulting from either mantle convection in the presence of

¹Department of Physics, University of Toronto, Toronto, ON M5S1A7, Canada. ²Department of Earth, Atmospheric, and Planetary Sciences, Massachusetts Institute of Technology, Cambridge, MA 02139, USA. ³Department of Geological Sciences, Brown University, Providence, RI 02912, USA.

*To whom correspondence should be addressed. E-mail: stanley@physics.utoronto.ca